Fluid Dynamics, Vol. 41, No. 5, 2006, pp. 795–809. Translated from Izvestiya Rossiiskoi Academii Nauk, Mekhanika Zhidkosti i Gaza, No. 5, 2006, pp. 135–151.

Vortex Formation Mechanisms in the Wake Behind a Sphere for $200 < \mathrm{Re} < 380$

V. A. Gushchin and R. V. Matyushin

Received February 1, 2006

Abstract — Direct numerical simulation and visualization of three-dimensional separated flows of a homogeneous incompressible viscous fluid are used to comprehensively describe different mechanisms of vortex formation behind a sphere at moderate Reynolds numbers ($200 \le \mathrm{Re} \le 380$). For $200 < \mathrm{Re} \le 270$ a steady-state rectilinear double-filament wake is formed, while for $\mathrm{Re} > 270$ it is a chain of vortex loops. The three unsteady periodic flow patterns corresponding to the $270 < \mathrm{Re} \le 290$, $290 < \mathrm{Re} \le 320$, and $320 < \mathrm{Re} \le 380$ ranges are characterized by different vortex formation mechanisms. Direct numerical simulation is based on the *Meranzh* (SMIF) method of splitting in physical factors with an explicit hybrid finite-difference scheme which possesses the following properties: second-order approximation in the spatial variables, minimal scheme viscosity and dispersion, and monotonicity. Two different vortex identification techniques are used for visualizing the vortex structures within the wake.

Keywords: incompressible viscous fluid, sphere, vortex formation mechanisms, wake, numerical simulation, visualization.

Studying the three-dimensional wakes behind bodies of finite dimensions in a homogeneous fluid flow is a conventional problem of fluid dynamics. In the flow past actual three-dimensional bodies, unsteady and three-dimensional separation zones of considerable interest are usually formed. Taking into account the high cost of laboratory experiments, the many additional factors, such as oncoming flow nonuniformity and surface roughness, which complicate the investigation and affect the flow pattern, and the continuing advances in computer technology (upgrading of performance and capacity) it is to be expected that our knowledge of separated flows obtained by numerical simulation on the basis of the complete fluid dynamics equations will only be extended and refined.

In this study, the flow of a homogeneous incompressible fluid in the wake behind a simple three-dimensional body (sphere) is numerically modeled at moderate Reynolds numbers $200 < \mathrm{Re} \le 380$; here, $\mathrm{Re} = W_0 d/\nu$, W_0 is the freestream velocity, d is the sphere diameter, and ν is kinematic viscosity. For many years, the main purpose of most experiments concerning the flow past a sphere has been to determine the sphere drag as a function of the Reynolds number [1]. Comprehensive experimental investigation of the sphere wake flow pattern was begun in [2] and continued in [3–12]. Nevertheless, so far an exhaustive description of the mechanisms of vortex formation in the sphere wake at moderate Re is still lacking. This paper makes an attempt to provide such a description.

In the figures reproduced in [2] the main elements of the wake are clearly visible; these are (1) a recirculation region immediately behind the sphere, (2) a shear layer between this region and the outer flow which constitutes a continuation of the boundary layer into the wake flow, and (3) the vortex structures of the wake. In [2] the sphere wake flow patterns were classified as follows: (1) $0 < \mathrm{Re} < 210$, single-filament wake (an axisymmetric recirculation (stagnation) region); (2) $210 < \mathrm{Re} < 270$, a rectilinear double-filament wake; (3) $270 < \mathrm{Re} < 290$, a wavy double-filament wake; (4) $290 < \mathrm{Re} < 410$, a chain of vortex loops; and (5) $290 < \mathrm{Re} < 700$, a double row of vortex rings (for $290 < \mathrm{Re} < 410$ different experimental sets gave

0015–4628/06/4105–0795

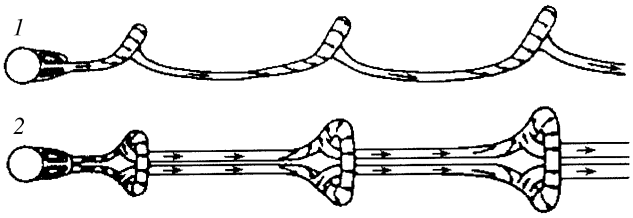

Fig. 1. Schematic representation of the sequence of vortex loops in the sphere wake for $300 < \mathrm{Re} < 420$ in the experiment [4]: *1*, side view and *2*, top view

different wake flow patterns). In [2] steady-state flows were formed for $\mathrm{Re} < 270$ and unsteady flows for $\mathrm{Re} > 270$.

In the experiments [3] transition from an axisymmetric single-filament wake to a steady-state non-axisymmetric double-filament wake was established at $\mathrm{Re} = 190$. Different authors attribute transition from the double-filament wake to an unsteady flow pattern to the $270 \le \mathrm{Re} \le 400$ range. Thus, in [4] the following features were noted: (1) for $\mathrm{Re} > 300$ hairpin-shaped vortex loops (Fig. 1) start to separate periodically with regular variation in intensity and frequency, thus forming laminar vortices up to $\mathrm{Re} = 800$ (on the Strouhal number range $0.15 < \mathrm{St} < 0.21$, where $\mathrm{St} = fd/W_0$ and f is the vortex separation frequency; (2) for $200 < \mathrm{Re} < 420$ all the loops are oriented to the same direction (upwards) and the symmetry of the wake about a plane is observable, which no longer exists for $\mathrm{Re} > 420$ when the loops in the wake are directed alternately to the right and to the left.

For the case of uniform $280 < \mathrm{Re} < 300$ flow past a sphere, in [5] the alternate irregular appearance of two vortex structures in the wake is established; these are pairs of wavy filaments and hairpin-shaped loops. For uniform $300 < \mathrm{Re} < 400$ flow in [5] the Strouhal number range is $0.125 < \mathrm{St} < 0.141$, which is narrower than that in [4] ($0.15 < \mathrm{St} < 0.17$). In [5] the vortex formation mechanism in the wake is described for $\mathrm{Re} = 375$ for the case in which the flow incident on the sphere has a vertical shear; the investigation used visualization of the shear layer and the vortex structures in the wake. In the flow two characteristic regions can be distinguished, namely, the upper (with a greater velocity) and lower parts of the shear layer enveloping the recirculation region. The mechanism of formation of a new hairpin-shaped loop can be broken up into three stages. First, the upper part of the shear layer extends downstream much more rapidly than the lower part; then its edge is rolled up around two vortex loops (stems of the first wake loop); and, finally, it is transformed into a new hairpin loop.

Thus, experimental investigations have made a great contribution to the study of sphere wake flow patterns for $\mathrm{Re} \le 380$. Starting from the eighties of the last century mathematical modeling began to be used for a more detailed study of vortex wakes downstream of a sphere [6, 7]. Researchers came up against the problem of visualizing the vortex structures in the wakes. Thus, in [6] a special visualization technique was used; it was based on instantaneous vorticity lines. For $\mathrm{Re} = 500$ and a $50 \times 100 \times 50$ difference grid the deformation of an axisymmetric vortex ring of the recirculation region to a closed loop carried away downstream was schematically represented. In [13] it was proposed to identify the vortex flow cores by plotting the surfaces $\mathrm{Im}(\sigma_{1,2}) = 0$, where $\mathrm{Im}(\sigma_{1,2})$ is the imaginary part of the complex-conjugate eigenvalues of the velocity gradient tensor.

In the nineties, new approaches to the visualization of the vortex flow core were developed [14] and the classification of the patterns of the flow past a sphere was further refined. In [14] it was proposed to identify the vortex flow cores by plotting the surfaces $\lambda_2 = 0$, where λ_2 is the second eigenvalue of a symmetric tensor representing the sum of the squares of the symmetric and antisymmetric parts of the velocity gradient tensor. In [8, 9, 15–17] transition to the double-filament wake was observed at $\mathrm{Re} = 211$, 210.5, 212, 210, and 250, respectively, and a further transition to an unsteady flow at $\mathrm{Re} = 270$, 297, 270 to 285, 277.5, and 375, respectively. In [8, 9] a poorly-known nontrivial fact was noted, namely, that the unsteady flow pattern (for $270 < \mathrm{Re} < 300$ in [8] and for $297 < \mathrm{Re} < 603$ in [9]) is characterized by a nonzero time-average

coefficient of the overall lateral force. In [8] by plotting the $\lambda_2 = 0$ surfaces for $\mathrm{Re} = 300$ it was shown that each hairpin-shaped loop observable in experiments [4] (Fig. 1) actually consists of two loops. In fact, let us cut in two the stems of the loop in Fig. 1. Then the right halves of these stems belong to the main, upward-oriented loop and the left halves to the induced, downward-oriented loop. The forward part of the induced loop, located below the imaginary boundary between the hairpin stems in Fig. 1, cannot be visualized by means of the technique used in [4]. In [18], as in Fig. 1, for the sphere wake flow at $\mathrm{Re} = 350$ only the upward-oriented loops are shown; in this case visualization was based on the construction of a surface $\mathrm{Im}(\sigma_{1,2}) \neq 0$ (the particular value of $\mathrm{Im}(\sigma_{1,2})$ is not mentioned in [18]). In [10–12] the λ_2-technique [14] was applied for identifying vortices; for $1 \leq \mathrm{Re} \leq 20.5$ and $20.5 < \mathrm{Re} \leq 200$, respectively, separationless and separated axisymmetric flows past a sphere were numerically obtained; for $200 < \mathrm{Re} \leq 270$ it was a rectilinear double-filament wake, for $270 < \mathrm{Re} < 420$ separation of the fixed edge of the vortex shell enveloping the recirculation region, accompanied for $360 < \mathrm{Re} < 400$ by slow regular rotation of the shell around the line of sphere motion; and for $400 \leq \mathrm{Re} \leq 600$ alternate separation of opposite edges of the vortex shell.

This shows that for $\mathrm{Re} \leq 380$ the results of mathematical modeling of the separated wake flows behind a sphere are in fairly good agreement with the experimental data; different techniques have now been developed for visualizing the vortices but the detailed mechanisms of vortex loop formation are still poorly understood. Accordingly, in this paper we shall make an attempt to arrive at such an understanding.

1. FORMULATION OF THE PROBLEM

We will consider the problem of incompressible viscous flow past a sphere; the fluid is assumed to be homogeneous and the flow uniform at infinity. The system of Navier-Stokes equations governing the flow is as follows:

$$\begin{aligned} &\frac{\partial \mathbf{v}}{\partial t} + (\mathbf{v}\nabla)\mathbf{v} = -\nabla p + \frac{2}{\mathrm{Re}}\Delta \mathbf{v}, \\ &\nabla \mathbf{v} = 0 \end{aligned} \tag{1.1}$$

where $\mathbf{v}$ is the velocity vector normalized by W_0, p is the pressure normalized by ρW_0^2, and ρ is the density.

Let x, y, z be Cartesian coordinates and (U, V, W) be the components of the velocity vector $\mathbf{v}$ in the directions x, y, z. It is assumed that the freestream velocity vector $(0, 0, W_0)$ is parallel to the z axis. Equations (1.1) are written in the spherical coordinate system R, θ, φ, where $x = R\sin\theta\cos\varphi$, $y = R\sin\theta\sin\varphi$, and $z = R\cos\theta$. Let u, v, w be the components of the velocity vector $\mathbf{v}$ in the directions R, θ, φ. The conditions of no-slip, $v = 0$ and $w = 0$, and impermeability, $u = 0$, are imposed on the spherical surface. On the outer boundary of the computation domain (spherical surface of radius R_N) the boundary conditions corresponding to the undisturbed flow, $u = \cos\theta$, $v = -\sin\theta$, and $w = 0$, are imposed for $z < 0$, and for $z \geq 0$ the conditions $u = \cos\theta$, $v = -\sin\theta$, and $\partial w/\partial R = 0$.

For the correct modeling of separated flows, the difference grid must be refined near the body surface in order to resolve the boundary layer. For this reason, the following transformation is introduced in the radial direction:

$$R_i = R(r_i) = 1 + \frac{i}{N_0}\sqrt{\frac{2}{\mathrm{Re}}} + \left(\frac{i}{N} r_{\max}\right)^m, \qquad i = 1 : N$$

where N_0 is the number of cells of the computation grid located within a boundary layer of thickness $\delta = \sqrt{2/\mathrm{Re}}$. In this work, in all the calculations we took $m = 3$ and $r_{\max} = 3$; therefore, $R_N \approx 14.5d$. Thus, the computation domain under consideration can be mapped onto the rectangular parallelepiped (r, θ, φ): $0 \leq r \leq r_{\max}$, $0 \leq \theta \leq \pi$, $0 \leq \varphi \leq 2\pi$ with a uniform $N \times M \times L$ grid inside it.

For modeling separated flows of a homogeneous incompressible viscous fluid governed by Eqs. (1.1) we used the *Meranzh*[1] method of splitting in physical factors with an explicit hybrid difference scheme for approximating the convective terms of the equations ensuring the second order of approximation in the spatial variables, minimal scheme viscosity and dispersion, normal operation over a wide Reynolds number range, and monotonicity [19–22].

The efficiency of the *Meranzh* (SMIF) method and the greater power of supercomputers make it possible adequately to model three-dimensional separated incompressible viscous flows past a sphere at moderate Reynolds numbers. Calculations were performed on the MBC-1000 multi-processor system (42 *Intel Xeon* 1.7 GHz processors).

2. VISUALIZATION OF THE VORTEX STRUCTURES IN THE SPHERE WAKE

For understanding the dynamics and the mechanisms of separation of the vortex structures of an incompressible viscous fluid in a sphere wake, the three well-known intuitive vortex indicators, namely, a pressure minimum, streamlines, and vorticity isosurfaces, do not suffice. Thus, in the simple case of axisymmetric $\mathrm{Re} = 100$ flow past a sphere, two vortex structures can be distinguished in the wake, namely, a ring in the recirculation region and a shell around the ring [9–12]. At the same time, in the sphere-fitted reference frame the streamlines can visualize only the ring and the $\boldsymbol{\omega} = 0.5\,\mathrm{curl}\,\mathbf{v}$ vorticity contours only the shell, while the pressure contours can visualize neither of the two [9–12].

Similarly, for a complicated three-dimensional flow, the vorticity magnitude isosurfaces indicate only some of the vortex structures in the flow rather than all of them (Fig. 2*a*). Therefore, special visualization techniques, which make it possible to visualize most of the wake vortices, have been proposed. We will briefly describe the essence of the two methods [13, 14] used in this study (Fig. 2*b* and *c*).

Let us fix a certain point in the flowfield and study the behavior of the streamlines in a Cartesian coordinate system $\mathbf{x} = (x, y, z)$ having its origin at this point and moving with its velocity. In the vicinity of this point (0, 0, 0) in the linear approximation we can write $\mathbf{v} = d\mathbf{x}/dt \approx \mathbf{T}\mathbf{x}$, where $\mathbf{T}$ is the velocity gradient tensor ($T_{ij} = v_{ij} = \partial v_i/\partial x_j$). If two eigenvalues σ_1 and σ_2 of the tensor $\mathbf{T}$ are complex-conjugate, that is, $\sigma_1 = \alpha - i\beta$ and $\sigma_2 = \alpha + i\beta$ ($\beta = \mathrm{Im}(\sigma_{1,2}) > 0$), then from the theory of ordinary differential equations it is known that two corresponding complex-conjugate eigenvectors $0.5(\mathbf{h}_1 \pm i\mathbf{h}_2)$ can be so chosen that they are composed of two real vectors $\mathbf{h}_1$ and $\mathbf{h}_2$ which form a plane, in which the phase trajectories are either closed ovals with a center at the fixed point (for $\alpha = 0$) or spirals with a focus at this point which indicates the presence of a vortex there [23]. In this case, the angular velocity of fluid rotation about this fixed point is equal to β. Thus, the vortex flow core has been defined as a set of flow subdomains with complex-conjugate eigenvalues of the velocity gradient tensor [13] (see the contours of $\mathrm{Im}(\sigma_{1,2}) > 0$ in Fig. 2*d* and the $\mathrm{Im}(\sigma_{1,2}) = 0.005$ surface in Fig. 2*c*, where, in view of the plane symmetry of the flow, only a half surface is shown).

In [14] the vortex flow core is defined as the set of flow subdomains with a negative second eigenvalue of the $\mathbf{S}^2 + \boldsymbol{\Omega}^2$ tensor ($\lambda_2 < 0$, Fig. 2*b* and *e*), where $\mathbf{S}$ and $\boldsymbol{\Omega}$ are the symmetric and antisymmetric parts of the velocity gradient tensor ($S_{ij} = 0.5(v_{i,j} + v_{j,i})$ are the strain rate tensor components and $\Omega_{ij} = 0.5(v_{i,j} - v_{j,i})$ are those of the vorticity tensor; the symmetric tensor $\mathbf{S}^2 + \boldsymbol{\Omega}^2$ possesses three real eigenvalues $\lambda_1 \geq \lambda_2 \geq \lambda_3$). The efficiency of this definition for visualizing certain actual three-dimensional incompressible flows was demonstrated in [14].

For plane flows we have $\sigma_{1,2} = \pm\sqrt{\lambda_2}$; therefore, the definitions of the vortex flow core proposed in [13] and [14] are equivalent. At the same time, for axisymmetric flows in the sphere wake the $\mathrm{Im}(\sigma_{1,2}) = 0$ surface envelops a greater volume than the $\lambda_2 = 0$ surface; however, the surfaces are similar in topology. In the recirculation region the extrema of the functions λ_2 and $\mathrm{Im}(\sigma_{1,2})$ approximately coincide with a singular point (center) of the streamline pattern in the sphere-fitted reference frame.

[1] *Meranzh* is the abbreviation for *MEtod RAsshchepleniya v Neszhimaemoii Zhidkosti* or Splitting Method for Incompressible Flows (SMIF).

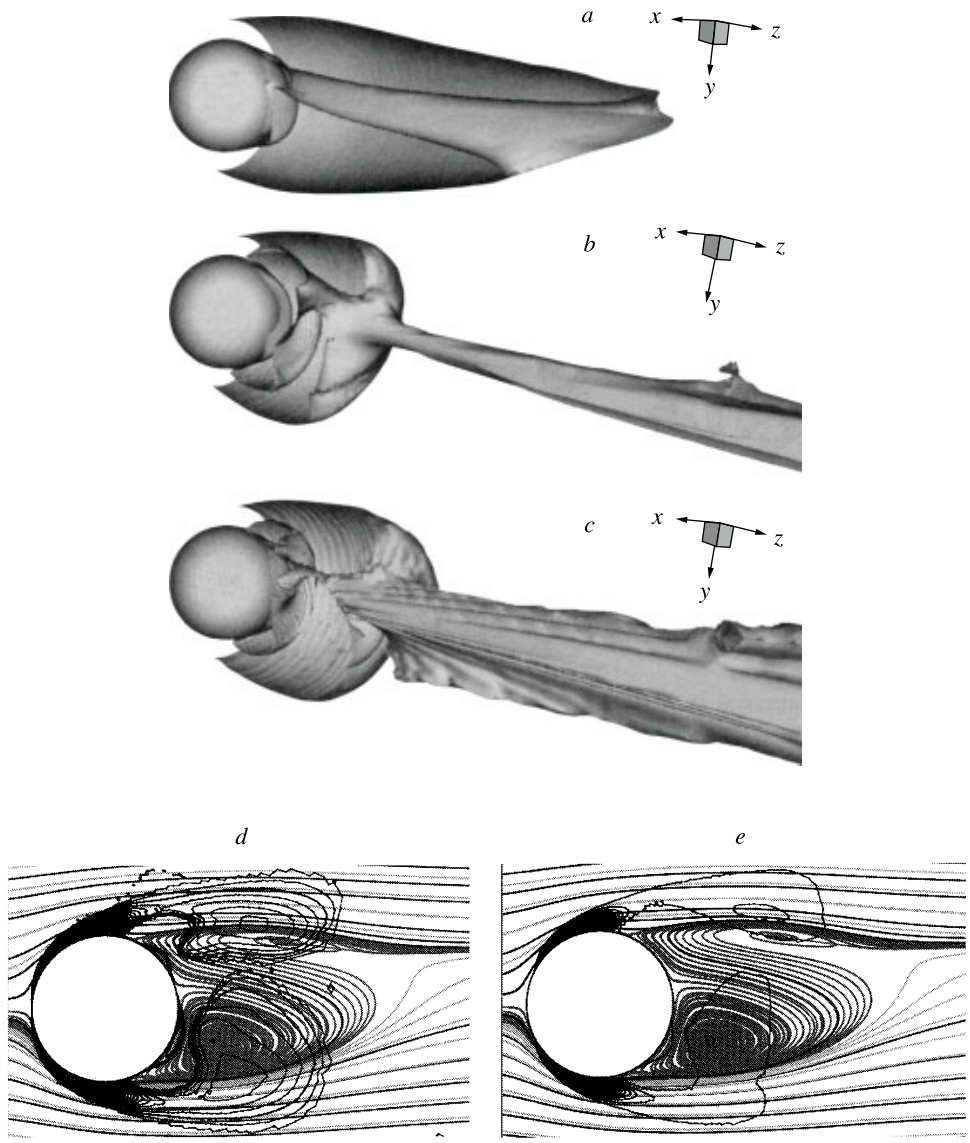

Fig. 2. Double-filament wake at Re = 250; *a* to *c* relate to the surfaces $|\boldsymbol{\omega}| = 0.2$ ($\boldsymbol{\omega} = 0.5 \cdot \operatorname{curl} \mathbf{v}$), $\lambda_2 = -2 \cdot 10^{-5}$, and $\operatorname{Im}(\sigma_{1,2}) = 0.005$; *d* and *e* relate to the isolines of $\operatorname{Im}(\sigma_{1,2}) > 0$ with a step of 0.006 and $\lambda_2 < 0$ with a step of 0.02 against the background of the streamlines in the plane of symmetry of the wake ($180 \times 90 \times 180$ grid)

3. METHODOLOGICAL AND TEST CALCULATIONS

For all the Reynolds numbers under consideration (Re $\leq$ 380) the axisymmetric flow corresponding to the axisymmetric boundary conditions is first calculated. In order to obtain a non-axisymmetric solution of system (1.1) for a chosen Re, a brief disturbance must be introduced into the calculated axisymmetric flowfield corresponding to this Re. The disturbance was taken in the form of a shear in the flow incident on the sphere; after it has been introduced, symmetry about a plane is established in the wake downstream of the sphere. The plane of symmetry of the wake passes through the line of body motion and the straight line along which the flow incident on the sphere is subjected to uniform shear. Thus, any initial orientation of this plane can be preassigned. With time, the plane of symmetry may turn through an arbitrary angle about the z axis and its position can be traced using, for example, the friction lines on the rear of the sphere (Fig. 3*b*). On the primary separation line in Fig. 3*b* the saddle *S* and nodal *N* critical points, through which the plane of symmetry of the wake passes, are clearly visible.

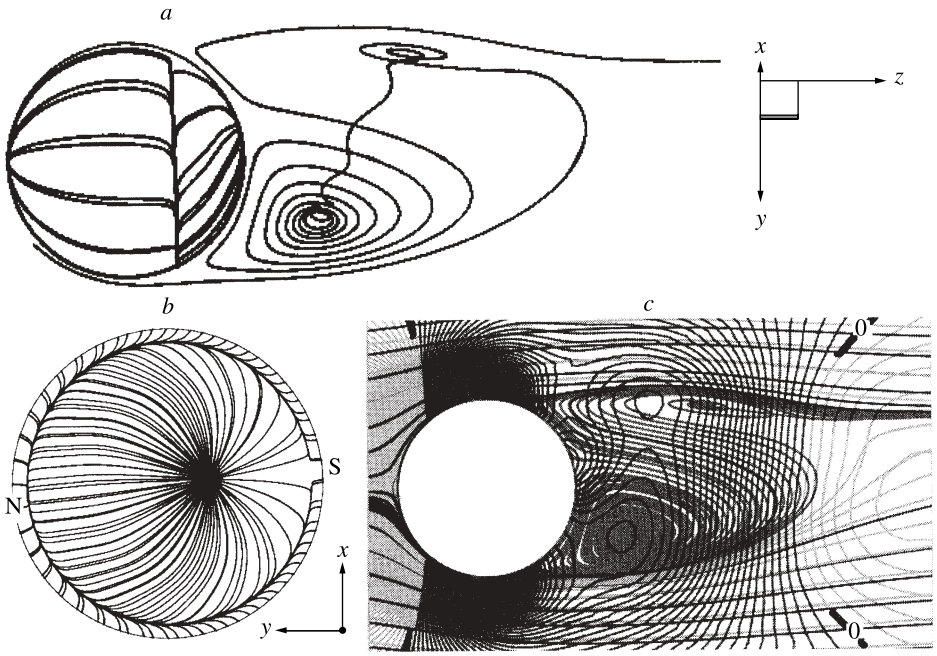

Fig. 3. Double-filament wake at Re = 250; *a* — three-dimensional streamline starting in the plane of symmetry of the wake; *b* — friction lines on the rear of the sphere; and *c* — pressure isolines with a step of 0.01 against the background of the streamlines in the plane of symmetry of the wake

The software package for homogeneous incompressible viscous flow past a sphere was comprehensively tested in [10, 11, 22], the results of the testing being found to be in good agreement with the experimental data and the calculations of other authors. The methodological calculations performed in [11] on $60 \times 36 \times 72$, $120 \times 60 \times 120$, and $180 \times 90 \times 180$ grids for Re = 250 showed that the flow topology is conserved (Fig. 2).

4. RECTILINEAR DOUBLE-FILAMENT WAKE ($200 < \mathrm{Re} \leq 270$)

For $20.5 < \mathrm{Re} \leq 200$ an axisymmetric steady-state recirculation region is formed in the sphere wake (in the streamline pattern in the sphere-fitted reference frame); this region is associated with a vortex ring in the $\mathrm{Im}(\sigma_{1,2}) > 0$ and $\lambda_2 < 0$ isoline patterns. In turn, the vortex shell of the wake in the same patterns is associated with the recirculation zone in the streamline pattern in the reference frame fitted to the oncoming flow. As Re increases from 20.5 to 200, the ring enlarges; the vortex shell approaches the ring, extends along the line of the sphere motion, and connects with the ring [10, 11]. Meanwhile, the fluid particle velocity in the ring increases and a local pressure minimum is formed in the recirculation region. For Re = 200 the local pressure minimum, the $\mathrm{Im}(\sigma_{1,2})$ maximum, and the λ_2 minimum in the recirculation region approximately coincide with each other and with the singular point (center) in the streamline pattern in the sphere-fitted reference frame. After a small short disturbance in the form of oncoming flow shear along the vertical x axis ($\partial W/\partial x > 0$) has been introduced into the calculated axisymmetric flow, the flow remains axisymmetric for $\mathrm{Re} \leq 200$, whereas for $\mathrm{Re} > 200$ the pressure is so redistributed along the vortex ring core that it becomes smaller in the lower than in the upper part of the ring. The fluid particles move along a spiral from top to bottom in the ring core and from bottom to top on the ring periphery.

Then the ring tilts and the stable upper focus in Fig. 3*a* corresponding to the upper part of the ring begins to be fed by fluid from the incident flow which has passed beneath the sphere (a streamline is twisted toward the center of a stable focus and untwisted away from the center of an unstable focus). In Fig. 3*a* the fluid flows from the upper focus along the ring core to the lower unstable focus and then, untwisting, flows away downstream enveloping the upper focus from the left and from above. Streamlines different

from the streamline in Fig. 3*a*, which originate in the flow incident on the sphere and pass near the primary separation line on the sphere, envelop the wing core along a spiral several times, rising upward, and then depart downstream forming two vortex filaments (Fig. 2*b* and *c*). Therefore, it may be concluded that these filaments are connected with the ring.

Then the wake transformation process ceases at $200 < \mathrm{Re} \leq 211$ and continues at $211 < \mathrm{Re} \leq 270$ (decaying azimuthal fluctuations occur in the recirculation region, see Section 5). Thus, at $100 < \mathrm{Re} \leq 270$ the axisymmetric wake transforms into a steady rectilinear double-filament wake (Figs. 2 and 3) characterized by the presence of a plane of symmetry and nonzero coefficients of the overall lateral force C_l and rotational moments ($C_l = \sqrt{C_x^2 + C_y^2}$, where C_x and C_y are the coefficients of the forces acting on the sphere along the x and y axes). The Re-dependence of C_l and the drag coefficient of the sphere C_d is given below.

Re	200	203	210	220	230	250	270
C_l	0.000	0.029	0.045	0.058	0.064	0.065	0.076
C_d	0.772	0.768	0.758	0.747	0.734	0.702	0.691

Let us consider the different ways of visualizing the double-filament wake vortex structure, as presented in Fig. 2. The vorticity magnitude surface (Fig. 2*a*) distinguishes neither the filaments nor the deformed ring in the wake. From a comparison of the λ_2 contours and the streamlines in the plane of symmetry of the wake (Fig. 2*e*) it is clear that the upper local minimum of λ_2 does not correspond to the upper stable focus in the streamline pattern but belongs to the wake shell. For this reason, for the correct perception of the vortex structure of the wake visualized using the $\lambda_2 = -2 \cdot 10^{-5}$ surface in Fig. 2*b*, this surface should be mentally cut in two by the streamplane proceeding from the primary separation line (Figs. 2*e* and 3*b*). Then one part corresponds to the wake shell and the other to the deformed ring. The cut line can be fairly clearly traced in the λ_2 and $\mathrm{Im}(\sigma_{1,2})$ surfaces (Fig. 2*b* and *c*).

In Fig. 2 the $\mathrm{Im}(\sigma_{1,2}) = 0.005$ surface envelops a larger space than the λ_2 isosurface. It also reveals a more complicated topology of the vortex structure in the recirculation region (Fig. 2*c* and *d*). In Fig. 2*d* three local maxima of $\mathrm{Im}(\sigma_{1,2})$ are observable in the plane of symmetry of the wake, of which two lie on the upper and lower boundaries of the recirculation region, while the third approximately coincides with the lower focus in the streamline pattern and the lower local pressure minimum (Fig. 3*c*). In Fig. 2*e* there are two local minima of λ_2, of which the upper belongs to the shell and the lower approximately corresponds to the lower focus in the streamline pattern. Therefore, the topologies of the $\mathrm{Im}(\sigma_{1,2})$ and λ_2 isosurfaces in Fig. 2 do not coincide. Since the function $\mathrm{Im}(\sigma_{1,2}$, as distinct from the function λ_2, has a clear physical meaning (see Section 2), it is preferable to use $\mathrm{Im}(\sigma_{1,2})$ isosurfaces for visualizing the three-dimensional vortex structures in the wake.

5. UNSTEADY WAVY DOUBLE-FILAMENT WAKE ($270 < \mathrm{Re} \leq 290$)

For $200 < \mathrm{Re} \leq 270$, once a disturbance has been introduced into the calculated axisymmetric flow, after a time a balance is established between the amounts of the fluid feeding the upper focus and passing along the deformed ring core and further downstream (Fig. 3*a*; see Section 4). For $\mathrm{Re} > 270$ this balance is not achieved; instead, a steady periodic process of formation of new links of the vortex loop sequence in the sphere wake can be observed ($\langle C_d \rangle = 0.683$, $\mathrm{St} = 0.133$, $\langle C_l \rangle = 0.079$, and the fluctuation amplitude $\Delta C_l = 0.0042$).

We will consider this process over a single period. We will begin with the moment $t = 1496.4$, when C_l is near-minimal. In Fig. 4*a* a shell enveloping the recirculation region, two upward-oriented main loops, and a downward-oriented induced loop can be discerned in the vortex structure. Let us trace the appearance of new induced and main loops during one period. First, two stems of the first main loop (two filaments proceeding from the recirculation region and connected with its ring) generate the forward part of the new induced loop in the external flow and extend downstream the lateral edges of the shell (Fig. 5*b*, 3*b* and 2*s*). At the same time, a new ring $R1$ is generated in the recirculation region due to the Kelvin-Helmholtz

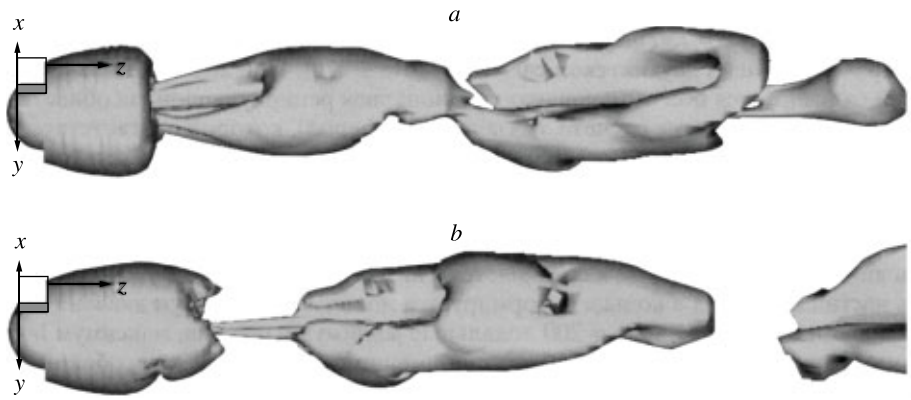

Fig. 4. Sequence of vortex loops in the sphere wake for Re = 280; $\mathrm{Im}(\sigma_{1,2}) = 0.02$ surfaces during a period: *a* and *b* relate to $t = 1496.4$ and 1504.4 ($120 \times 60 \times 120$ grid)

shear instability (Figs. 5 and 6*a*); for $t = 1498.4$ the upper part of $R1$ vanishes and for $t = 1498.9$ reappears (Figs. 5 and 6*b*).

Then the restored new ring develops and occupies the place of the gradually vanishing previous ring of the recirculation region (Figs. 5 and 6*c* and *d*). In the instantaneous streamline pattern, this process is characterized by enlargement of the upper focus (the upper part of the new ring) due to its also being fed with fluid that has passed above the sphere (Fig. 6*d* and *a*). At the same time, the development of the restored new ring is accompanied by the formation of new filaments connected with it (Fig. 5*c*, 1*f*) and the generation of an embryo of the forward part of the incipient (new main) loop in the external flow (above the first loop stems, Fig. 5*c*, 3*t*). As the new filaments connected with the new ring develop, the connection between the first loop stems and the vanishing previous ring of the recirculation region ceases to exist (Fig. 5*c*). Then the upper edge of the shell rolls up, separates, and vanishes (Figs. 5*d* (2*t*), and 6, *c* and *d*), thus terminating the formation of the new main loop (Fig. 5, *d* and *a*).

In the periodic process described above five main mechanisms of vortex formation can be distinguished; they operate in three different flow regions, namely, the recirculation region $D1$, the shell $D2$, and the outer flow $D3$. They are:

(1*k*) ring (or half-ring) generation in $D1$ near the spherical surface due to the Kelvin-Helmholtz shear instability (Figs. 5 and 6*a*);

(1*f*) formation of two filaments in $D1$ (stems of an incipient loop) connected with this ring (Fig. 5, *c* and *d*);

(2*s*) downstream extension of the lateral edges of the shell $D2$ (Fig. 5*b*);

(2*t*/*b*) rolling up and separation of the upper or lower edges of $D2$ (Figs. 5 and 6, *c* and *d*); and

(3*t*/*b*) generation in $D3$ of the forward part of the upward- or downward-oriented loop.

Processes 2*s*, 2*t*, 2*b*, 3*t*, and 3*b* are induced by filaments proceeding from $D1$.

Thus, for $270 < \mathrm{Re} \leq 290$ the detailed mechanism of vortex formation in the sphere wake during one period can be written in symbolic form as $\mathrm{M}\{1k\text{–}\,2s\text{–}1k\text{–}3b\}\text{–}\{1f\text{–}3t\text{–}2t\}$, where the curly brackets indicate the mechanisms operating in the first and second halves of the period. On the Re range under consideration, in experiments [2, 5] a wavy double-filament wake corresponding to the filaments in Figs. 4 and 5 was observable. The forward parts of the wake loops were not visible in experiments [2, 5], which involved using dye particles starting from the spherical surface, since they were induced in the outer flow rather than separating from the shell edges.

Returning to the comparison of the two techniques for visualizing vortices in the wake, it should be noted that for $270 < \mathrm{Re} \leq 290$ the λ_2-technique is unable to identify the upper part of the $R1$ ring [11].

We will now return to the rectilinear double-filament wake or, to be more precise, to its process of formation (see Section 4). Whereas for $200 < \mathrm{Re} \leq 211$ the axisymmetric ring deforms after a disturbance has been introduced and the subsequent flow structure does not change with time, for $211 < \mathrm{Re} \leq 270$ a set

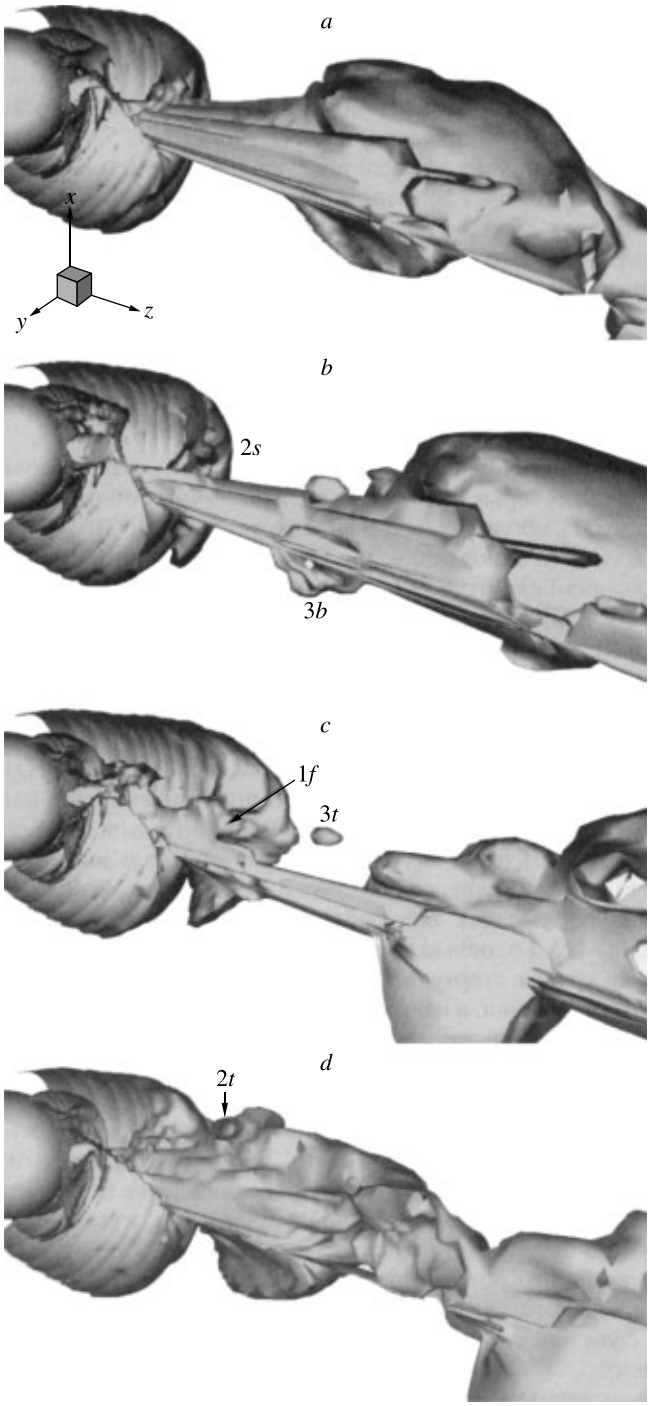

Fig. 5. Near wake at Re = 280; $\mathrm{Im}(\sigma_{1,2}) = 0.005$ surfaces during a period: *a* to *d* relate to $t = 1496.4$, 1500.4, 1504.4, and 1507.4; the flow regions where the main vortex formation mechanisms 1*f*, 2*s*, 2*t*, and 3*t*/*b* operate, are marked

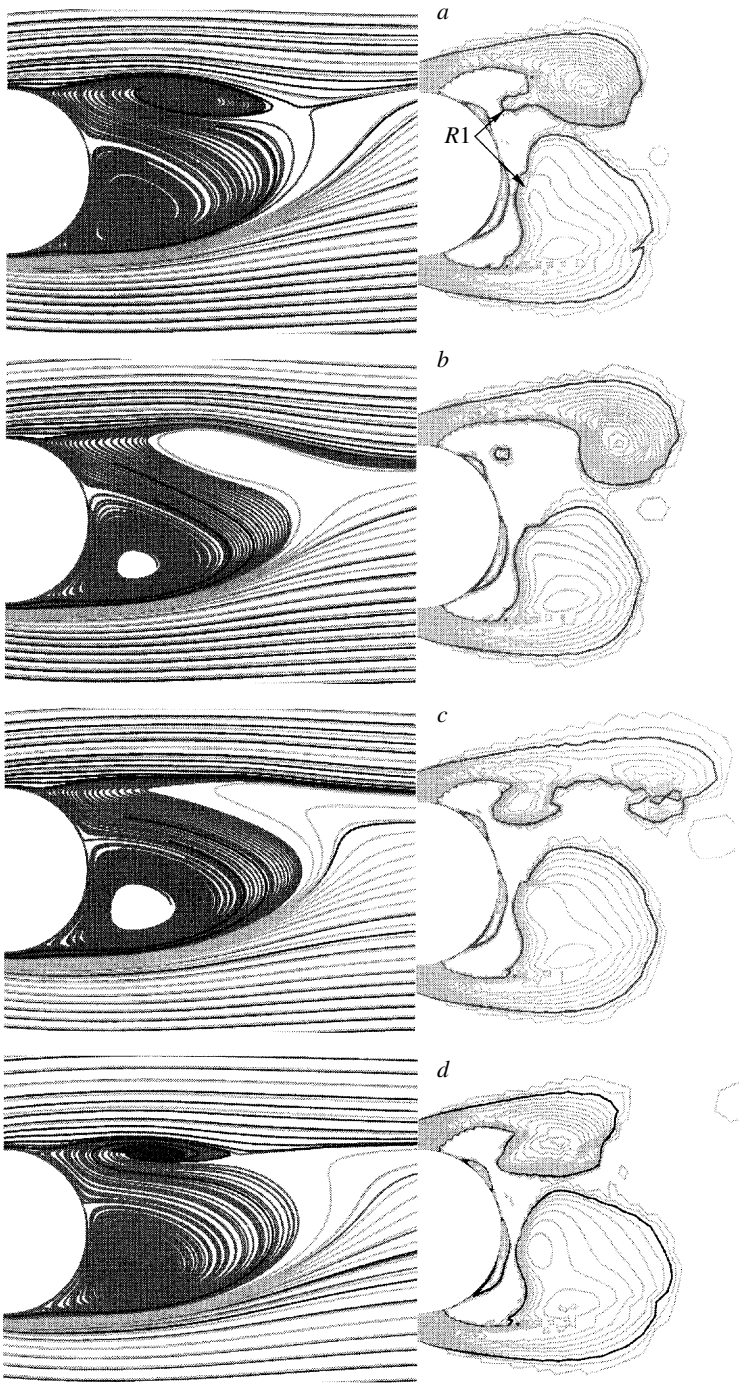

Fig. 6. Instantaneous streamlines and isolines of $\mathrm{Im}(\sigma_{1,2}) > 0$ with a step of 0.04 in the plane of symmetry of the wake at $\mathrm{Re} = 280$; *a* to *d* relate to $t = 1496.4$, 1500.4, 1504.4, and 1507.4

of new rings is generated in the recirculation region after the initial deformation of the axisymmetric ring. This periodic process decays with time and can be described as M$\{1k$–$2s$–$1k$– $3b\}$–$\{1f$–$3t\}$, since the upper edge of the shell does not separate. The duration of this approach to the steady state increases with Re (three new rings are generated for Re = 250 and 35 rings for Re = 270).

6. DETAILED VORTEX FORMATION MECHANISM AT Re = 350

We will now consider the detailed mechanism of formation of the new induced and main loops during a single period at Re = 350 (Fig. 7, $\langle C_d \rangle = 0.627$, St = 0.133, $\langle C_l \rangle = 0.068$, and $\Delta C_l = 0.033$). We will again start from the moment $t = 882$ when C_l is near-minimal.

Due to the similarity of the loop formation mechanisms for Re = 320 and 350 over the larger part of the period, we will use Fig. 8 (Re = 320) for the further demonstration of the process occurring at Re = 350.

At $t = 882$ a new $R1$ ring is generated (Figs. 7 and 8a (1k)), whose upper part has already vanished at $t = 883.5$. For Re = 350 the sizes of the upper and lower foci in the instantaneous streamline patterns in the plane of symmetry of the wake are naturally larger than those for Re = 280 (Fig. 6a). Moreover, at $t = 882$ the fluid that has passed below the sphere does not flow into the recirculation region due to the formation in this region of a second new ring $R2$ (Fig. 8b) connected with the stems of the first main loop. These stems form a new induced loop, thus extending the lateral shell edges downstream (Fig. 7a (2s)). The stems of the new induced loop are connected with the main ring of the recirculation region (Fig. 7b).

Next the upper part of the $R2$ ring generates a new third half-ring $R3$ in the upper part of the recirculation region and vanishes (Figs. 7b and 8c). Then the $R3$ half-ring connects with the shell (Fig. 7c), while the induced loop stems form in the outer flow an embryo of the forward part of the incipient (new main) loop and extend the lateral edges of the shell downstream (Fig. 7c and d (3t and 2s)), while the upper part of the main ring of the recirculation region splits into two parts, of which the left part drifts toward the sphere and connects with the shell (Fig. 7c and d (1d)) transforming into the new fourth ring. Now the new induced loop stems are connected with the right half of the main ring, while the development of the new fourth ring is accompanied by the formation of filaments (stems of the incipient (new main) loop) connected with the fourth ring (Fig. 7d (1f)). At the same time, the rolling up and separation of the upper edge of the shell are also observable (Fig. 7d (2t)).

Thus, at Re = 350 the detailed mechanism of vortex formation in the sphere wake during a single period can be described in symbolic form as $M\{\langle 1k\rangle$–$2s$–$1k$–$\langle 1k\rangle\}$–$\{\langle 2s\rangle$–$1d$–$\langle 1f$–$3t$– $2t\rangle\}$; here, the angle brackets contain the mechanisms which are also observable for Re = 280. For Re = 350 using the λ_2-technique for visualizing the vortex structure dynamics in the wake gives the same detailed mechanism [10, 11]. Here, a new (sixth) main vortex formation mechanism has appeared, namely:

(1d) drift of the main ring of the recirculation region toward the sphere (Fig. 7c and d).

In spite of the numerous complicated processes that occur in the recirculation region at Re = 350, the pattern of the instantaneous friction lines on the rear of the sphere varies only slightly during a period. Only insignificant oscillations of the rear stagnation point take place (Fig. 3b). Methodological calculations carried out for Re = 350 on different grids ($60 \times 36 \times 72$, $120 \times 60 \times 120$, and $180 \times 90 \times 180$) showed that the flow topology and the detailed vortex formation mechanism are conserved.

In the experiments [4] conducted for $300 < \mathrm{Re} < 420$ the forward parts of the induced loops (directed downward in Fig. 7b) were not visualized (Fig. 1) and the stems of these loops were taken for the continuations of the stems of the main loops (directed upward in Fig. 7b). Approximately the same effect can be observed in the present study when considering isosurfaces with the greater value $\mathrm{Im}(\sigma_{1,2}) = 0.05$. With account for this remark, the vortex flow topology in the sphere wake obtained for Re = 350 coincides with that presented in Fig. 1. The integral flow characteristics for Re = 350 are also in good agreement with those obtained in [1, 4, 5].

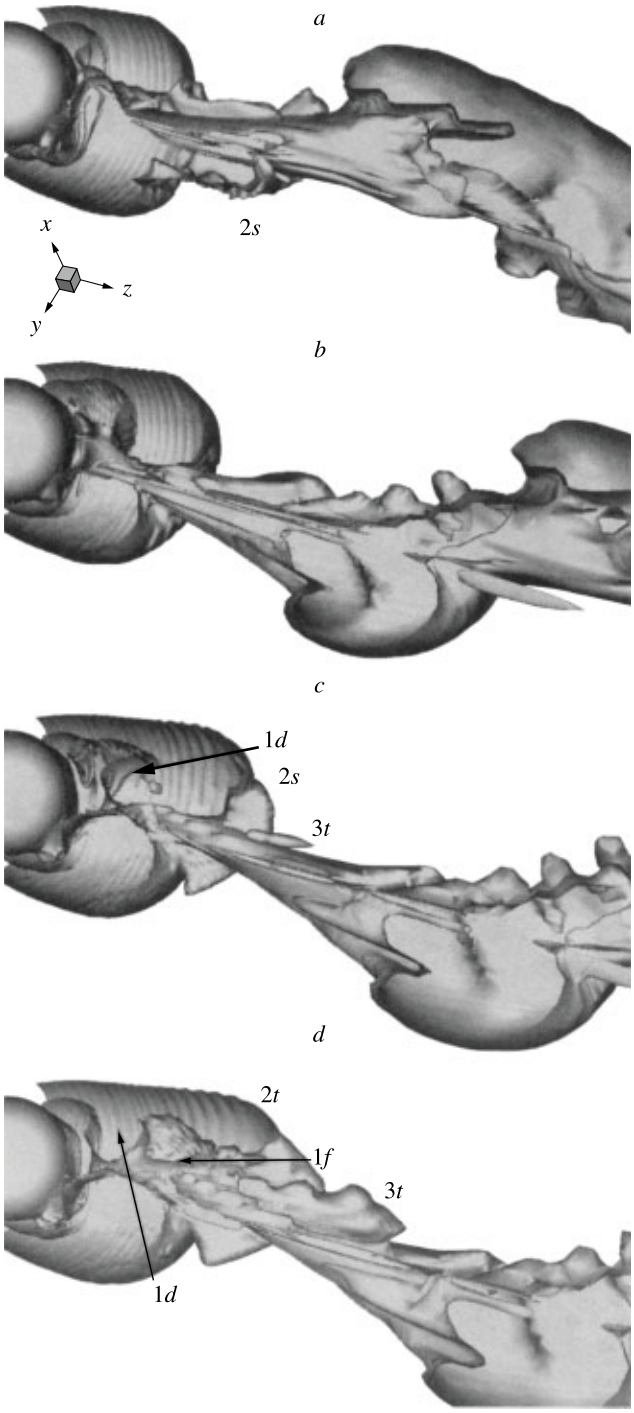

Fig. 7. Near wake at Re = 350; $\mathrm{Im}(\sigma_{1,2}) = 0.02$ surfaces during a period: *a* to *d* relate to $t = 882$, 886.5, 889.5, and 891 ($180 \times 90 \times 180$ grid); the main mechanisms 1*d*, 1*f*, 2*s*, 2*t*, and 3*t* are marked

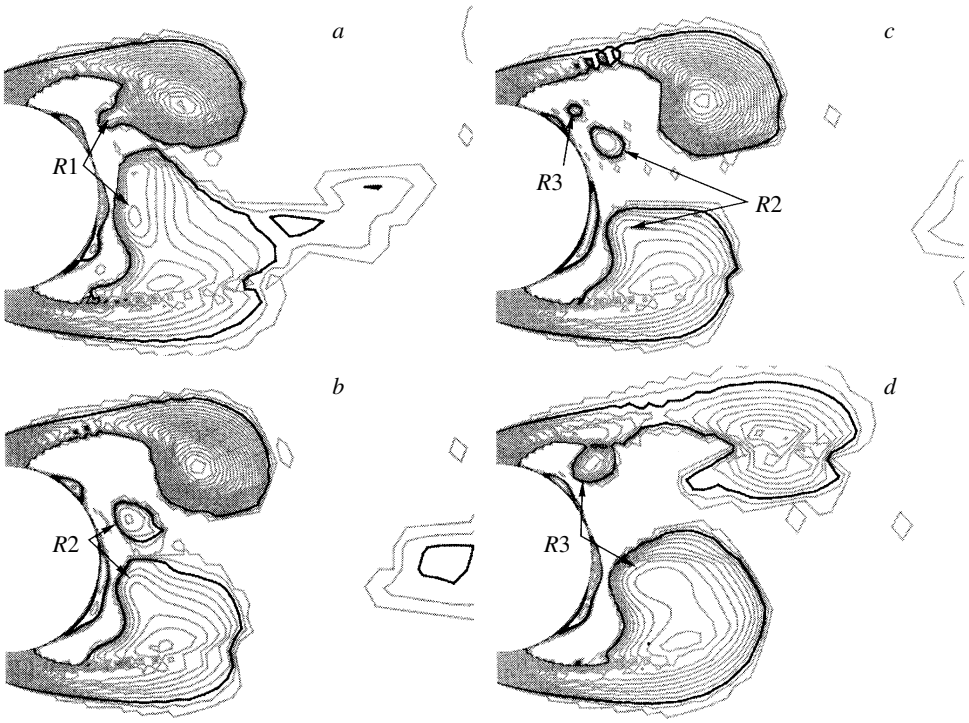

Fig. 8. Near wake behind the sphere at Re = 320; $\mathrm{Im}(\sigma_{1,2} > 0)$ isolines with a step of 0.04 in the plane of symmetry of the wake during a period: *a* to *d* relate to $t = 453$, 455, 456.5, and 460 ($120 \times 60 \times 120$ grid)

7. THREE UNSTEADY FLOW PATTERNS AT $270 < \mathrm{Re} \leq 380$

As the Reynolds number increases from 270 to 380, the vortex formation mechanism changes considerably (see Table 1). For Re = 290 during a time interval $\Delta t \approx 1$ a second new ring is observable. With further increase in the Reynolds number up to Re = 320 the upper part of the second new ring enlarges and generates a third new ring, which later transforms into the main ring (Fig. 8*c* and *d*). In this case, the 3*b* mechanism is replaced by 2*s*, since the induced loop is formed starting from its forward part for $270 < \mathrm{Re} \leq 290$ (see Section 5) and from the stems for $290 < \mathrm{Re} \leq 320$ (see Section 6). For Re = 320 an incipient drift of the left part of the main ring toward the sphere can be observed (1*d* mechanism, Fig. 8*d*).

Thus, the vortex formation mechanisms are essentially different for $270 < \mathrm{Re} \leq 290$, $290 < \mathrm{Re} \leq 320$, and $320 < \mathrm{Re} \leq 380$. In other words, a new flow pattern is detected for $290 < \mathrm{Re} \leq 320$, since previously it was believed that the same flow pattern was realized over the entire $290 < \mathrm{Re} \leq 380$ range [2, 4, 5]. The new flow pattern is characterized by the periodic formation of a second new ring in the recirculation region. This ring is connected with the stems of the first main loop of the wake, while the stems of the induced loop in process of formation are connected with the main ring of the recirculation region. Therefore, starting from Re = 290 four filaments proceeding from the recirculation region can be periodically observed (Fig. 7*b*), whereas for $270 < \mathrm{Re} \leq 290$ only two filaments can be visualized (Fig. 5). For $320 < \mathrm{Re} \leq 380$ part of the main ring is periodically displaced toward the sphere; with further increase in the Reynolds number the induced loops become "doubles" of the main loops (their mechanisms formation become the same, that is, during a period the $M\{\langle 2s\rangle\text{–}1d\text{–}1k\text{–}\langle 1f\text{–}3b\text{–}2b\rangle\}\text{–}\{\langle 2s\rangle\text{–}1d\text{–}1k\text{–}\langle 1f\text{–}3t\text{–}2t\rangle\}$ mechanism is realized .

For $270 < \mathrm{Re} < 375$ symmetry about a plane can be observed in the sphere wake. In this case, the time-average coefficients of the overall lateral force $\langle C_l \rangle$ and the rotational moment $\langle C_{T,y} \rangle$ about a line passing through the sphere center and perpendicular to the plane of symmetry of the wake, are different from zero (for example, at Re = 360 we have $\langle C_l \rangle = 0.084$ and $\langle C_{T,y} \rangle = 0.0068$). For $375 \leq \mathrm{Re} \leq 380$ the shell starts

Table 1

Re	M1	M2	Figure
[270, 290]	$\langle 1k–2s–1k\rangle–3b$	$\langle 1f–3t–2t\rangle$	5 and 6
290	$\langle 1k\rangle–1k–\langle 2s–1k\rangle–3b$	$\langle 1f–3t–2t\rangle$	–
[290, 320]	$\langle 1k\rangle–2s–1k–\langle 1k\rangle$	$\langle 2s\rangle–\langle 1f–3t–2t\rangle$	8
[320, 380]	$\langle 1k\rangle–2s–1k–\langle 1k\rangle$	$\langle 2s\rangle–1d–\langle 1f–3t–2t\rangle$	7

to rotate slowly around the line of motion of the sphere ($St_{rot} = 0.0054$ and 0.0088 for $Re = 375$ and 380, respectively). Similar rotation with $St_{rot} = 0.0067$ was numerically modeled in [24] for $Re = 420$. Thus, the plane symmetry of the wake vanishes at $Re = 375$, whereas in experiments [4, 5] it disappeared at $Re = 420$. Therefore, for $Re < 375$ we can speak of the similarity of the calculated and experimental [4, 5] topologies of the vortex structure of the wake (Fig. 1). For $Re < 375$ the values of the time-average coefficients C_d and C_l and the Strouhal number St are also in good agreement with the data [1, 4, 5]:

Re	270	280	290	300	320	350	360	375	380
St	0.125	0.133	0.140	0.145	0.148	0.133	0.150	0.183	0.183
$\langle C_l\rangle$	0.076	0.079	0.082	0.084	0.086	0.068	0.084	0.082	0.083
$\langle C_d\rangle$	0.691	0.683	0.675	0.669	0.654	0.627	0.630	0.622	0.619

For $Re = 350$ the calculations made on a finer $180 \times 90 \times 180$ grid give better agreement with the experimental data. The increase in the Strouhal number to 0.183 obtained for $375 \le Re \le 380$ is due to the uniform rotation of the shell, that is, the loss of the plane symmetry of the wake. A similar sharp increase in the Strouhal number was also observable in experiments [4, 5] with loss of the plane symmetry of the wake at $Re > 420$.

Summary. Uniform homogeneous incompressible viscous flow past a sphere is mathematically modeled at moderate Reynolds numbers $200 \le Re \le 380$. The system of Navier-Stokes equations governing the flow is solved using the explicit difference *Meranzh* (SMIF) method. For visualizing the vortex structure of the wake, isosurfaces of two functions are plotted, namely, the imaginary part of the complex-conjugate eigenvalues of the velocity gradient tensor **T** and the second eigenvalue of a symmetric tensor representing the sum of the squares of the symmetric and antisymmetric parts of the tensor **T**.

The different vortex formation mechanisms in the wake behind a sphere are described in detail. Thus, a steady rectilinear double-filament wake is formed when $200 < Re \le 270$ and a sequence of vortex loops when $Re > 270$. The three unsteady periodic flow patterns for $270 < Re \le 290$, $290 < Re \le 320$, and $320 < Re \le 380$ are characterized by different vortex formation mechanisms, the main difference being observable in the recirculation region of the wake. When $290 < Re \le 320$ a new flow pattern is detected, since it was previously believed that the same flow pattern is realized over the entire $290 < Re \le 320$ range. The vortex formation process during a single period can be presented in the form of a sequence of six main mechanisms operating in three different flow regions, namely, the recirculation region $D1$, the vortex shell $D2$ enveloping $D1$, and the outer flow $D3$. These mechanisms are (1) ring (or half-ring) generation in $D1$; (2) formation in $D1$ of two filaments connected with this ring; (3) drift of the main ring in $D1$ toward the sphere; (4) downstream extension of the lateral edges of the $D2$ shell; (5) separation of the upper or lower edge of $D2$; and (6) generation in $D3$ of the forward part of an upward- or downward-oriented loop. The flows under consideration are characterized by plane symmetry (for $200 < Re < 375$) and nonzero time-average coefficients of the overall lateral force (lift) and the rotational moment about a line passing through the sphere center and perpendicular to the plane of symmetry of the wake. This unique property of the flow can be used in practice. As the Reynolds number increases from 270 to 380, the amplitude of the periodic azimuthal fluctuations in the recirculation region increases, which leads to the loss of plane symmetry at

Re = 375. The calculated results are in good agreement with the experimental data and the calculations of other authors.

The study was carried out with the support of the Russian Foundation for Basic Research (projects Nos. 05-01-00496 and 04-01-08021), the Program "Mathematical Modeling" of the Presidium of the Russian Academy of Sciences, and Program no. 3 of Basic Research of the Division of Mathematical Sciences of the Russian Academy of Sciences.

REFERENCES

1. F. W. Roos and W. W. Willmarth, "Some experimental results on sphere and disk drag," *AIAA J.*, **9**, 285 (1971).
2. R. H. Magarvey and R. L. Bishop, "Transition ranges for three-dimensional wakes," *Canad. J. Phys.*, **39**, 1418 (1961).
3. I. Nakamura, "Steady wake behind a sphere," *Phys. Fluids*, **19**, 5 (1976).
4. H. Sakamoto and H. Haniu, "A study on vortex shedding from spheres in a uniform flow," *Trans. ASME: J. Fluid Engng.*, **112**, 386 (1990).
5. H. Sakamoto and H. Haniu, "The formation mechanism and shedding frequency of vortices from a sphere in uniform shear flow," *J. Fluid Mech.*, **287**, 151 (1995).
6. S. Shirayama and K. Kuwahara, "Patterns of three-dimensional boundary layer separation," *AIAA Paper*, No. 0461 (1987).
7. U. Dallmann and B. Schulte-Werning, "Topological changes of axisymmetric and non-axisymmetric vortex flows," in: *IUTAM Symposium on Topological Fluid Mechanics, August 1989, Cambridge, UK* (1989).
8. T. A. Johnson and V. C. Patel, "Flow past a sphere up to a Reynolds number of 300," *J. Fluid Mech.*, **378**, 19 (1999).
9. V. A. Gushchin, A. V. Kostomarov, P. V. Matyushin, and E. R. Pavlyukova, "Direct numerical simulation of the transitional separated fluid flows around a sphere and a circular cylinder," *J. Wind Eng. & Industr. Aerodynamics*," **90**, 341 (2002).
10. V. A. Gushchin and P. V. Matyushin, "Classification of the patterns of separated flows around a sphere at moderate Reynolds numbers," in: *Mathematical Modeling. Problems and Results* [in Russian], Nauka, Moscow (2003), p. 199.
11. P. V. Matyushin, "Numerical simulation of three-dimensional separated flows of a homogeneous incompressible viscous fluid around a sphere," Thesis submitted for the degree of Candidate of Sciences, Moscow (2003).
12. V. A. Gushchin, A. V. Kostomarov, and P. V. Matyushin, "3D visualization of the separated fluid flows," *J. Visualization*, **7**, 143 (2004).
13. M. S. Chong, A. E. Perry, and B. J. Cantwell, "A general classification of three-dimensional flow fields," *Phys. Fluids*, **A2**, 765 (1990).
14. J. Jeong and F. Hussain, "On the identification of a vortex," *J. Fluid Mech.*, **285**, 69 (1995).
15. A. G. Tomboulides, "Direct and large-eddy simulation of wake flows: flow past a sphere," PhD Thesis, Princeton Univ. (1993).
16. R. Natarajan and A. Acrivos, "The instability of the steady flow past spheres and disks," *J. Fluid Mech.*, **254**, 323 (1993).
17. S. Lee, "A numerical study of the unsteady wake behind a sphere in a uniform flow at moderate Reynolds numbers," *J. Computers and Fluids*, **29**, 639 (2000).
18. R. Mittal and F. M. Najjar, "Vortex dynamics in the sphere wake," *AIAA Paper*, No. 3806 (1999).
19. O. M. Belotserkovskii, V. A. Gushchin, and V. N. Kon'shin, "Splitting method for studying stratified flows with free surfaces," *Zh. Vychisl. Mat. Mat. Fiz.*, **27**, 594 (1987).
20. V. A. Gushchin and V. N. Konshin, "Computational aspects of the splitting method for incompressible flow with a free surface," *J. Computers and Fluids*, **21**, 345 (1992).
21. O. M. Belotserkovskii, *Numerical Modeling in Continuum Mechanics* [in Russian], Fizmatlit, Moscow (1994).
22. V. A. Gushchin and P. V. Matyushin, "Numerical modeling of three-dimensional separated flows around a sphere," *Zh. Vychisl. Mat. Mat. Fiz.*, **37**, 1122 (1997).
23. L. S. Pontryagin, *Ordinary Differential Equations* [in Russian], Nauka, Moscow (1974).
24. V. Karlo and T. Tezduyar, "3D computation of unsteady flow past a sphere with a parallel finite element method," *Comput. Methods Appl. Mech. Engng.*, **151**, 267 (1998).